HHS Public Access

Author manuscript

Sci Transl Med. Author manuscript; available in PMC 2017 December 11.

Published in final edited form as:

Sci Transl Med. 2017 January 11; 9(372): . doi:10.1126/scitranslmed.aag2809.

Pharmacological rescue of diabetic skeletal stem cell niches

Ruth Tevlin[1,2], **Eun Young Seo**[1,2,*], **Owen Marecic**[1,2,*], **Adrian McArdle**[1,2,*], **Xinming Tong**[3,*], **Bryan Zimdahl**[2], **Andrey Malkovskiy**[4], **Rahul Sinha**[2], **Gunsagar Gulati**[2], **Xiyan Li**[5], **Taylor Wearda**[1,2], **Rachel Morganti**[2], **Michael Lopez**[2], **Ryan C. Ransom**[2], **Christopher R. Duldulao**[1], **Melanie Rodrigues**[1], **Allison Nguyen**[2], **Michael Januszyk**[1], **Zeshaan Maan**[1], **Kevin Paik**[1], **Kshemendra-Senarath Yapa**[1], **Jayakumar Rajadas**[4], **Derrick C. Wan**[1], **Geoffrey C. Gurtner**[1], **Michael Snyder**[5], **Philip A. Beachy**[6,7], **Fan Yang**[3,8], **Stuart B. Goodman**[8], **Irving L. Weissman**[2,9], **Charles K. F. Chan**[1,2,9,‡,†], and **Michael T. Longaker**[1,2,‡,†]

[1]Hagey laboratory for Pediatric Regenerative Medicine and Department of Surgery, Stanford University, Palo Alto, CA 94305, USA

[2]Institute for Stem Cell Biology and Regenerative Medicine, Stanford University, Palo Alto, CA 94305, USA

[3]Department of Bioengineering, Stanford University, Palo Alto, CA 94305, USA

[4]Department of Bio-materials and Advanced Drug Delivery, Stanford University, Palo Alto, CA 94305, USA

[5]Department of Genetics, Stanford University, Palo Alto, CA 94305, USA

[6]Depanment of Biochemistry, Stanford University, Palo Alto, CA 94305, USA

[7]Howard Hughes Medical Institute, Stanford, CA 94305, USA

[‡]Corresponding author. chazchan@stanford.edu (C.K.F.C.); longaker@stanford.edu (M.T.L.).
[*]These authors contributed equally to this work as co-second authors.
[†]These authors contributed equally to this work as co-senior authors.

SUPPLEMENTARY MATERIALS

www.sciencetranslationalmedicine.org/cgi/content/full/9/372/eaag2809/DC1

Materials and Methods
Fig. S1. MST apparatus and assessment.
Fig, S2. Impaired mSSC. and BCSP-mediated bone healing is consistent in multiple mouse models of DM.
Fig. S3. Resting glucose and weight between types of Db and pre-Db mouse models.
Fig. S4. Circulating IL-1b is elevated in both uninjured and injured Db mice.
Fig. S5. Local delivery of Ihh restores impaired bone healing in Db mice.
Fig. S6. Bone regeneration is impaired in Db versus WT mice, but osteoclastic activity is not notably affected.
Fig. S7. Neutralization of TNFα signaling in Db serum restores Ihh expression in cocultured mSSC.
Table S1. Primer sequence for qRT-PCR
Reference (42)

Author contribution: R.T. designed and porformod experiments, analyzed data, and wrote the manuscript E.Y.S. and O.M. performed experiments, and analyzed data, and edited the manuscript. A. McArdle performed experiments and analyzed data. X.T. made the hydrogels. R.S., G.G., and R.M. analyzed RNA-seq data. B.Z., A. Malkovskiy, X.L., T.W., M.L., C.R.D., and A.N. performed experiments. M.R., R.C.R., M.J., Z.M., K.P., K.-S.Y., and J.R. analyzed data. D.C.W., G.C.G., M.S., P.A.B., and F.Y. assisted in the design of the study. S.B.G. provided femoral head specimens. I.L.W. supervised the project, C.K.F C. supervised the project, designed and performed experiments, analyzed data, and wrote the manuscript. M.T.L supervised the project and edited the manuscript.

Competing interests: The authors, including I.L.W. declare that they have no equity holdings that relate to the topic of this paper, Patent is pending for the use of hedgehog agonists to address Specific hedgehog-related pathologies in diabetes

Data and materials availability: The data for this study have been deposited in the National Center for Biotechnology Information Gene Expression Omnibus database.

[8]Department of Orthopaedic Surgery, Stanford University, Palo Alto, CA 94305, USA

[9]Departments of Pathology and Developmental Biology, Stanford University, Palo Alto, CA 94305, USA

Abstract

Diabetes mellitus (DM) is a metabolic disease frequently associated with impaired bone healing. Despite its increasing prevalence worldwide, the molecular etiology of DM-linked skeletal complications remains poorly defined. Using advanced stem cell characterization techniques, we analyzed intrinsic and extrinsic determinants of mouse skeletal stem cell (mSSC) function to identify specific mSSC niche-related abnormalities that could impair skeletal repair in diabetic (Db) mice. We discovered that high serum concentrations of tumor necrosis factor-α directly repressed the expression of Indian hedgehog (Ihh) in mSSCs and in their downstream skeletogenic progenitors in Db mice. When hedgehog signaling was inhibited during fracture repair, injury-induced mSSC expansion was suppressed, resulting in impaired healing. We reversed this deficiency by precise delivery of purified Ihh to the fracture site via a specially formulated, slow-release hydrogel. In the presence of exogenous Ihh, the injury-induced expansion and osteogenic potential of mSSCs were restored, culminating in the rescue of Db bone healing. Our results present a feasible strategy for precise treatment of molecular aberrations in stem and progenitor cell populations to correct skeletal manifestations of systemic disease.

INTRODUCTION

Diabetes mellitus (DM) is a chronic metabolic disease that is increasing in frequency at an unprecedented rate (1–3). It is associated with a myriad of clinical complications, one of the most debilitating being impaired bone healing (4–8). Although patients with DM have increased bone resorption and osteoclast activity, how specific bone stem and progenitor cells contribute to the molecular etiology of DM-related skeletal complications is not well understood We set out to characterize molecularly the skeletal stem cell niche to elucidate the mechanism of impaired diabetic (Db) bone healing.

Our laboratory's recent identification of the mouse skeletal stem cell (mSSC), a single multipotent stem cell capable of producing all of the skeletal elements, enables us to determine the homeostatic and injury-induced phenotypes of the mSSC and its downstream lineage in Db mice (9). We showed previously that the mSSC and its downstream progenitor —the bone, cartilage, and stromal progenitor (BCSP)—facilitate the rapid repair of skeletal tissue in non-Db mice. When these cell types are reduced in number, fracture healing is severely impaired (9, 10). Thus, we tested whether aberrant stem and progenitor cell activity could lead to impaired Db bone healing.

RESULTS

mSSC-dependent skeletal repair is impaired in Db mice

To determine whether DM is associated with impaired fracture healing in mice, we created transverse femoral fractures in 10-week-old Db (Leprdb, denoted as DbLR) and non-Db

(C57Bl/6, denoted as WT) female mice and fixed them with an intramedullary pin (Fig. 1A). The Leprdb mouse is a model of type 2 DM and results from an autosomal recessive mutation of the *lepr* gene, which codes for the leptin receptor. These mice are hyperphagic and secrete excessive insulin, making them obese, insulin-resistant, hyperinsulinemic, and hyperglycemic from 4 weeks of age (11). We assessed bone healing using a variety of techniques, including mechanical strength testing (MST), histology, and high-resolution micro–computed tomography (μCT). MST of healing femora was conducted at post-fracture week 4 (fig. S1). This analysis revealed that healing DbLR femora were significantly weaker than healing WT controls (Fig. 1B). In addition, analysis of post-fracture week 4 callus with ex vivo μCT showed that DbLR femora had lower trabecular bone density than WT controls (Fig. 1C). Similarly, histomorphometric comparison of healing DbLR and WT femora showed reduced osteogenesis in DbLR mice; however, osteoclastic activity within the healing fractures was not significantly different between DbLR and WT mice (fig. S6).

To further test whether impaired bone healing in DbLR mice was associated with DM, we created femoral fractures in DbLR mice at postnatal week 4, before the onset of DM (denoted as pre-DbLR), This experiment allowed us to determine the effect of DM and aberrant leptin signaling (12, 13) on injury-induced bone regeneration. MST analysis showed no significant difference in strength between healing femora from pre-DbLR and age- and sex-matched controls (fig. S2A). These results indicate that impaired bone regeneration arose during active DM and was not related to aberrant leptin signaling. We also tested our hypothesis in streptozotocin-induced (DbSTZ) and diet-induced obesity (DbDIO) mouse models of DM. In both models of DM, the strength of healing femora was reduced significantly compared to WT controls (fig. S2B). Collectively, these findings show that DM impairs bone healing in multiple models of diabetes in mice.

Considering our previous characterization of mSSC- and BCSP-dependent skeletal growth and repair (Fig. 1D) (9, 10, 14), we hypothesized that a reduction in these cell populations could impair bone healing in DbLR mice. When we analyzed mSSC and BCSP populations isolated from uninjured femora of DbLR and WT mice using FACS, there was no significant difference in absolute cell numbers of either population (fig. S2C). When we assessed the injury-induced expansion of mSSCs and BCSPs within DbLR and WT calluses at post-fracture days 3, 7, 14, 21, and 28 (Fig. 1E), there was no significant difference in proportion of the total population for either cell type (Fig. 1F). However, absolute numbers of both mSSCs and BCSPs were significantly reduced in post-fracture day 7 calluses of DbLR mice (Fig. 1G). This result is interesting because post-fracture day 7 is a time point previously shown to exhibit maximal mSSC and BCSP expansion in non-Db mice (9, 10).

We also observed significantly lower absolute numbers of mSSCs and BCSPs in post-fracture day 7 calluses of DbDIO and DbSTZ mice but not in pre-DbLR mice compared to age- and sex-matched WT controls (fig. S2, D to F). Together, these results show that mSSC and BCSP injury-induced expansion is diminished in several mouse models of DM only when DM is active.

We next tested whether differences in cellular proliferation or apoptosis contributed to the deficient stem and progenitor injury response. To assess proliferative activity, we

administered BrdU, an intracellular label of rapidly dividing cells, to DbLR and WT mice 12 hours before FACS analysis on post-fracture day 3. We found that the percentage of BrdU-labeled mSSCs was significantly lower in DbLR calluses on post-fracture day 3 (Fig. 1H). We then assessed apoptotic activity in mSSCs from post-fracture day 7 calluses using FACS to analyze surface phosphatidylserine staining (measured with FITC-conjugated annexin V). mSSCs from DbLR calluses had greater apoptotic activity than those from WT controls (Fig. 1I). Thus, decreased proliferation and increased apoptotic activity of mSSC5 contribute to the deficient stem and progenitor injury response in Db mice.

Exposure to non-Db circulation does not rescue Db fracture healing

Given that exposure to blood circulated from a young animal enhances bone repair in aged animals (15) and that exposure to non-Db circulation improves Db cutaneous wound healing (16), we next investigated how exposure to non-Db blood affects Db bone healing. We joined age-and sex-matched mice in parabiosis in the following chimeric pairs: WT/DbLR, DbLR/DbLR, and WT/WT (Fig. 2A). Blood chimerism was confirmed at post-parabiosis week 4 (Fig. 2B). At post-parabiosis week 8, glycemic control was not changed in DbLR mice exposed to WT circulation or vice versa (Fig. 20). We then created a transverse femoral fracture fixed with an intramedullary pin in each animal of a parabiotic pair and assessed bone healing by MST at post-fracture week 4 (Fig. 2A). MST showed no significant difference in strength between WT femora of WT/DbLR and WT/WT pairs or between Db femora from WT/DbLR and DbLR/DbLR pairs (Fig. 2D). Furthermore, DbLR femur strength remained significantly lower than that of WT animals, indicating that exposure to circulating blood from a non-Db animal does not rescue Db fracture repair.

Cell-extrinsic factors impair mSSC-dependent bone healing in Db mice

Having seen reduced expansion of mSSCs after injury in Db mice and that exposure to a non-Db circulation does not rescue healing, we questioned whether intrinsic stem or progenitor cell dysfunction im-paired Db bone healing. To assess intrinsic cell activity, FACS-sorted mSSCs (2×10^4) from post-fracture day 7 calluses of DbLR or WT mice were transplanted separately beneath independent kidney capsules of non-Db, immunodeficient mice (Fig. 3A) (17). After 4 weeks, heterotopic skeletal grafts were explanted. We hypothesized that if DbLR mSSCs were intrinsically dysfunctional, then they would produce grafts of a different size and/or composition than those produced by WT mSSCs Histological analyses determined that the grafts were not significantly different in size (Fig. 3B, far left column) or composition (Fig. 3B, second column from left), suggesting that mSSC-dependent skeletogenesis is not constrained by cell-intrinsic factors in DbLR mice.

We next investigated whether mSSCs are affected by cell-extrinsic factors by transplanting each population (2×10^4), isolated from the appendicular skeleton of uninjured WT mice at postnatal day 3 (P3), beneath the kidney capsules of either DbLR or WT mice. We hypothesized that if cell-extrinsic factors impaired heterotopic bone formation, then grafts derived in DbLR mice would differ in size or composition from those in WT mice. Histomorphometric analyses revealed that grafts derived in DbLR mice differed significantly in size from those in WT mice (Fig. 3, B and C, right panel). These results suggest that cell-

extrinsic factors, potentially mediated by skeletal niche signaling, after mSSC skeletogenic potential and could provide a mechanism of impaired Db bone healing.

Molecular characterization of the skeletal niche points to therapeutic strategies

To identify molecular changes in skeletal niche signaling that could alter stem and progenitor activity in DbLR mice, we compared the transcriptomes of mSSCs and BCSPs from DbLR and WT mice using gene chip analysis of extracted mRNA. Each cell population was isolated from uninjured femora and post-fracture day 7 calluses. To elucidate differential gene expression, we analyzed our results using the Gene Expression Commons, a system designed by our laboratory to normalize experimental results against publicly available microarray data (18).

Given the importance of hedgehog (Hh) signaling in skeletal development (19–22), we questioned whether Hh signaling factors could be differentially expressed during the injury response in DbLR and WT mice. Notably, Indian hedgehog (Ihh) (a secreted Hh signaling molecule) (Fig. 4Ai, first row, black arrow), Smoothened (Smo) (a mediator of Hh signal transduction) (Fig. 4Ai, fifth row, black arrow), and Gli1 (an effector of Hh signaling) (Fig. 4Ai, sixth row, black arrow) were down-regulated in post-fracture day 7 DbLR calluses relative to WT controls. Western blot protein quantification reinforced these findings in FACS-sorted mSSCs isolated from the post-fracture day 7 calluses of DbLR and WT mice (Fig. 4B). We also analyzed the expression of Hh signaling factors in DbDIO and DbSTZ mice and found that mSSCs from post-fracture day 7 calluses also showed down-regulated Ihh and Smo expression relative to those from WT mice (Fig. 4C). Notably, this effect was not seen in mSSCs from post-fracture day 7 calluses of pre-DbLR mice, which instead had expression patterns resembling those of their age- and sex-matched non-Db controls (Fig. 4C). These results indicate that Hh signaling is altered in multiple mouse models of active DM.

In contrast, the expressions of other essential skeletogenic genes, such as *WNT* and *bone morphogenetic protein* (*BMP*), were not significantly altered in post-fracture day 7 Db mSSCs (Fig. 4Aii). We also found that genes involved in apoptosis were up-regulated and genes involved in cellular proliferation were down-regulated in post-fracture day 7 DbLR mSSCs and BCSPs (Fig. 4A, iii and iv).

To investigate whether Hh signaling is essential for mSSC-dependent osteogenesis, we antagonized Hh signaling in post-fracture day 7 WT mSSCs in vitro using XL139, a small-molecule antagonist of Smo. We then assessed bone formation using alizarin red staining, a marker of extracellular matrix mineralization, and found a dose-dependent reduction in the osteogenic potential of mSSCs treated with XL139 (Fig. 4D).

To verify that Hh antagonism impairs fracture repair in vivo, we administered XL139 to WT mice via oral gavage immediately after injury and assessed healing femur strength at post-fracture week 4 using MST. We found that femur strength was reduced significantly in XL139-treated versus untreated mice (Fig. 4E). We then isolated mSSCs and BCSPs from post-fracture day 7 calluses of XL139-treated versus untreated mice and found a highly significant reduction in the number of mSSCs and BCSPs after Hh antagonism (Fig. 4F).

To understand why Hh expression was repressed specifically in the skeletal niches of Db mice, we first performed proteomic analyses on DbLR and WT serum to identify systemic factors that could disrupt niche signaling. We found significantly higher levels of glucose and inflammatory cytokines such as tumor necrosis factor–α (TNFα) and interleukin-1b (IL-1b) in DbLR mice (Fig. 4G, TNFα; fig. S3, glucose; fig. S4, IL-1b). Single-cell RNA sequencing (scRNA-seq) revealed that TNFα receptors are coexpressed with Ihh, Ptch1, and Gli1 on both mSSCs and BCSPs isolated from post-fracture day 7 calluses of DbLR mice (Fig. 5, A to D).

To determine whether high levels of glucose or TNFα could directly repress Hh expression in skeletal niches, we cultured FACS-sorted mSSCs and BCSPs from uninjured P3 WT femora in glucose-supplemented, TNFα-supplemented, or control medium for 48 hours. We then measured Ihh expression using quantitative reverse transcription polymerase chain reaction (qRT-PCR) and found that Ihh expression was significantly reduced in both mSSC and BCSP cultures supplemented with TNFα but not in mSSC cultures supplemented with glucose (Fig. 5, E to G). The inhibition of Ihh expression by glucose in BCSPs suggests that TNFα alters Hh signaling at the stem cell level, whereas glucose alters Hh signaling in the stem cell's downstream progenitors. This TNFα-mediated repression of Ihh expression was dose-dependent in BCSPs (Fig. 5H). Furthermore, neutralization of TNFα with anti-TNFα antibodies restored Ihh expression levels in mSSCs cultured in DbLR serum (fig. S7). Cumulatively, these data indicate that systemically elevated levels of TNFα could suppress Ihh signaling, potentially disrupting essential pro-skeletogenic autocrine and/or paracrine cross-talk between mSSCs and BCSPs (Fig. 5, I and J).

Ihh and Gli1 expression are repressed in Db human skeletal progenitors

Because Db patients also exhibit high levels of TNFα, we investigated whether human Db skeletal progenitors also exhibit repressed Ihh signaling. Because fracture callus tissue from Db patients is difficult to obtain, we used freshly dissected femoral and knee specimens from osteoarthritic Db patients undergoing total joint arthroplasty. These tissues had large regions of cartilage degeneration that we used to investigate reparative signaling in isolated skeletogenic cells purified by FACS (Fig. 6A). We found that about 30% of the nonhematopoietic ($CD45^-$) and nonendothelial ($CD31^-$ and $Tie2^-$) fraction of these cells expressed CD146, a marker that has been used previously to describe a population of human skeletal stem and progenitor cells (Fig. 6B) (23). Gene expression analysis confirmed that both Ihh and Gli1 are down-regulated in Db patient samples relative to non-Db patients, consistent with our findings in mice (Fig. 6, C and D).

Local delivery of Ihh rescues Db fracture healing

We then assessed whether modulating local Hh expression could improve Db fracture repair by applying degradable poly(ethylene glycol) hydrogels coated with recombinant Ihh, Sonic hedgehog (Shh), or phosphate-buffered saline (PBS) control to the defect sites of DbLR or WT mice immediately after fracture creation (Fig. 7A). Notably, MST analyses of healing femora harvested at post-fracture week 4 revealed that Ihh- and Shh-treated DbLR femora were significantly stronger than PBS-treated controls (Fig. 7B). To determine whether this improvement was associated with changes in mSSC or BCSP activity, we profiled the

cellular composition of Hh-treated and untreated post-fracture day 7 calluses using FACS and found that the absolute numbers of both mSSCs and BCSPs increased significantly in Hh-treated calluses (Fig. 7C). We also found that FACS-sorted mSSCs isolated from Hh-treated calluses of DbLR mice formed significantly more colonies in vitro than mSSCs from DbLR controls. These results indicate that local delivery of Hh to the skeletal stem cell niche rescued DbLR mSSC clonal activity, emphasizing the importance of Hh signaling to mSSC activity (Fig. 7D).

To gain insight into how exogenous Hh treatment stimulated mSSC and BCSP activity, we assessed the proliferation and apoptosis in each population after treatment. We found that BrdU uptake was significantly higher in mSSCs and BCSPs in post-fracture day 3 calluses after Hh treatment in DbLR mice (Fig. 7E). We also found that Hh treatment reduced the apoptotic activity of DbLR mSSCs relative to controls, as assessed by annexin V expression. By comparison, it did not affect the apoptotic activity of WT mSSCs (Fig. 7F). Together, these results suggest that Hh treatment improves the mSSC and BCSP injury response in part by enhancing cellular expansion and survival in calluses of DbLR mice.

We then investigated whether Hh treatment could enhance mSSC- and BCSP-mediated osteogenesis. Both mSSCs and BCSPs from Hh-treated, post-fracture day 7 calluses were more osteogenic than those from DbLR controls, as assessed in vitro by alizarin red staining (Fig. 7G) (24). These results are supported by histomorphometric analyses that show significantly enhanced osteogenesis in DbLR mice (fig. S5).

Together, these findings demonstrate that targeted molecular therapy corrects specific skeletal niche defects caused by systemic Db disease, resulting in the restoration of mSSC-dependent repair in DbLR mice (Fig. 8).

DISCUSSION

Here, we describe a new mode of stem cell therapy that treats the altered reparative function of local stem and progenitor cells in Db mice. In systemic diseases with multiple complications, it is challenging to characterize the mechanisms of tissue-specific dysfunction. Our approach determined cell-intrinsic versus cell-extrinsic control of skeletogenesis based on the recent characterization of the mSSC and its downstream progenitors that produce skeletal tissue (9). Under normal conditions, mSSCs and BCSPs facilitate rapid healing. However, in Db mice, significantly reduced injury expansions of mSSCs and BCSPs suppressed osteogenesis and impaired healing. Several groups have reported that exposure to a young circulation rejuvenates muscle, heart, brain, and skeletal tissue (15, 25–27) and that exposure to a non-Db circulation improves Db cutaneous wound healing (16). However, we found that exposure to a non-Db circulation did not restore Db bone healing. As a result, we centered our investigation on the mSSC and its downstream progenitors.

Deviations in normal mSSC activity could be cell-intrinsic, or they could arise from alterations to the external regulatory niche environment. Because heterotopic transplantation of mSSCs or BCSPs from Db and WT calluses revealed that the intrinsic skeletogenic

activity of each cell population did not differ, we hypothesized that cell-extrinsic abnormalities in skeletal niche signaling impaired Db healing. Heterotopic transplantation of WT mSSCs and BCSPs into Db or WT mice supported this hypothesis because the size of grafts produced in Db mice was significantly reduced. Factors associated with mSSC niche signaling include BMP, WNT, Hh proteins, and transforming growth factor–β. We examined these factors within the mSSC niche of Db mice to identify abnormalities that could impair healing and ultimately lead to effective intervention.

Our laboratory previously investigated paracrine- and autocrine-mediated control of normal mSSC activity with gene expression analysis and scRNA-seq (9, 21). When we applied the same analysis to Db mSSCs, we found that, although many skeletogenic signaling pathways were unchanged, Hh signaling was altered in Db mSSCs after fracture. Ihh signaling is essential for embryonic skeletal formation and endochondral ossification, and it has also been implicated in regulation of cartilage development (28). Our results indicate that Hh signaling is also necessary for skeletal regeneration in mice and suggest that decreased Ihh expression in Db calluses is likely a major factor in the molecular etiology of poor fracture healing in DM. In addition to skeletal stem and progenitors in mice, we observed repressed Ihh signaling in human skeletal progenitors isolated from femoral head and knee specimens of Db patients (Fig. 6). These results indicate that Hh signaling and its importance to postnatal skeletal repair appear to be conserved between mouse and humans.

We also found that elevated levels of TNFα in Db mice can directly suppress Ihh expression in mSSCs and BCSPs. TNFα is expressed by a wide variety of tissues, including macrophages, T cells, and adipose tissue. Although TNFα plays a key role in mediating the inflammatory response against microbial infections, it has also been implicated in autoimmune disease and diabetes. In addition, the development of insulin resistance in multiple mouse models of diabetes (29) is believed to occur in part through TNFα-mediated inhibition of insulin receptor activity in muscle and fat cells (30). In humans, elevated levels of TNFα are frequently detected in Db patients and have been shown to disrupt fracture healing (31–34). Thus, our findings suggest that diminished Ihh signaling plays a mechanistic role in the chronic inflammatory state associated with DM (35).

Because anti-TNFα antibody therapy may lead to increased adiposity and the absence of TNFα may impair fracture repair (36, 37), we instead chose to directly modulate skeletal niche signaling by delivering recombinant Ihh or Shh to the local fracture site using a slow-release hydrogel. We found that both Ihh and Shh restored fracture repair in Db mice, in part by enhancing mSSC expansion, survival, and osteogenic potential in Db calluses. Because we observed that skeletal progenitors in bone and cartilage tissues isolated from DM patients undergoing total joint arthroplasty also show down-regulation of Ihh and Glil expression, it is possible that local administration of recombinant Ihh or small-molecule Hh agonists will also accelerate fracture repair in these patients. However, additional preclinical and clinical studies are necessary to Identify the appropriate delivery strategy and to validate the safely and efficacy of localized Hh stimulation as treatment for both chronic and acute skeletal injuries in DM patients.

Kayal *et al.* reported that streptozotocin-induced type 1 DM led to increased osteoclast activity during fracture healing (38). However, in a model of type 2 DM, they observed that osteoclastogenesis was decreased (39). These findings are inconsistent with our observation that osteoclast activity was not significantly changed in vivo in models of type 2 DM, suggesting that additional factors could influence the activity of the regenerative niche during skeletal healing.

In summary, we devised a feasible strategy for reversing complex, tissue-specific pathologies associated with metabolic disease. We demonstrate that the local application of two factors, Ihh and Shh, rescues Db bone healing by stimulating the mSSC expansion seen after injury. Thus, by determining how DM affects the mSSC and its supporting niche, we could identify a molecular therapy that can be identified and used to treat metabolic disease directly at the stem cell level.

Although our findings are consistent in multiple models of DM, the recent identification of type 2 diabetes subgroups emphasizes that multifactorial diseases can exhibit diverse patient phenotypes (40). Thus, the mechanisms described in the current study may not apply to all cases of DM. However, precision medicine techniques that isolate single cells from tissue-specific populations obtained from individual patients could provide new routes for treating complications of metabolic disease. Because the Hh signaling pathway is well conserved in vertebrates, we anticipate that Hh-mediated molecular therapies that directly target stem cells in human Db patients could be therapeutic.

MATERIALS AND METHODS

Study design

The objective of this study was to understand the cellular and molecular mechanisms underlying impaired bone healing in Db mice. Multiple mouse models of diabetes were used and are described in the “Animals” section of the Supplementary Materials. For all experiments, the number of samples analyzed is outlined in the figure legends, and each experiment was performed in triplicate. Further statistical information is outlined in the “Statistical analysis” section. No outliers have been excluded from our analysis. Animals used for the Hh rescue experiments were randomized with animals receiving hydrogel alone, hydrogel with Ihh, or hydrogel with Shh.

Femoral fractures

Ten-week-old mice were anesthetized with aerosolized isoflurane. Analgesia was administered, and the surgical site was prepared before skin incision, A medial parapatellar incision was created. The patella was dislocated laterally to expose the femoral condyles. The medullary cavity was reamed using a 23- to 25-gauge, 0.64 to 0.51 OD (mm), 15 mm length regular bevel needle (BD) before insertion of an intramedullary pin of equal diameter into the medullary cavity. A transverse, mid-diaphyseal fracture was made using scissors. The pin remained in situ to provide relative stability during healing. The patella was relocated, muscles were reapproximated, and the skin was closed using a 6-0 nylon suture. Animals were radiographed to verify fracture alignment and assess fracture fixation.

Animals with fracture displacement were excluded. Pin diameter was adjusted according to femoral cavity lumen diameter to minimize migration (41)

Isolation of skeletal progenitor cells

Uninjured and fractured femora were harvested at post-fracture days 3, 7, 10, 14, 21, and 28. Fracture calluses were dissected using microscopy. Tissues were crushed with mortar and pestle in collagenase buffer [collagenase (2.2 mg/ml), deoxyribonuclease, 1 M $CaCl_2$; (1000x), p188 (100x), 1 M Hepes (50x), Medium199] and heated to 37°C for 10 min to activate collagenase. Each sample underwent three serial digestions at 37°C for 25 min under gentle agitation, Dissociated cells were filtered through a 40-μm nylon mesh and washed in FACS buffer (2% fetal bovine serum in PBS). Each sample was pelleted at 200*g* at 4°C and resuspended in FACS buffer. Then, each sample was layered onto a Histopaque gradient before centrifugation at 1400 rpm for 15 min at room temperature with zero acceleration. The cloudy interphase was aspirated, washed with FACS buffer, and centrifuged. The cells were stained with fluorochrome-conjugated antibodies against CD45, Ter119, Tie2. α_V integrin, Ly 51, CD105, Thy1.1, and Thy1.2 for purification by flow cytometry. Cells were sorted twice (once on "yield," then on "purity") to increase purity (BD FACSAria).

Isolation of human bone progenitors

Femoral heads were obtained from Db and non-Db patients undergoing total joint arthroplasty. Cells from areas of cartilage degeneration were processed as described in the "Isolation of skeletal progenitor cells" section. Cells were stained with fluorochrome-conjugated antibodies against CD45, CD235, and CD146 for purification by flow cytometry. Cells were sorted twice (once on yield, then on purity) (BD FACSAria). Human skeletal progenitors were defined as $CD45^{-}CD235^{-}CD146^{+/-}$.

Statistical analysis

All analyses were performed using GraphPad Prism, Data were analyzed using two-tailed Student's *t* test and/or one-way ANOVA and Tukey post hoc correction. Statistical significance was assigned for $P \leq 0.05$. All experiments were done in triplicate.

Supplementary Material

Refer to Web version on PubMed Central for supplementary material.

Acknowledgments

We thank B. Myers, R. Mann, N. Quarto, and S. Li for mentorship; S. Kantoff. L. Quinn, K. Moore, and T storm for laboratory management; A. McCarty and F. Manuel for animal care; S. Jensen for assistance with surgical technique and animal care; P. Lovelace and J. Ho In the Stanford Shared FACS Facility; T. Doyle in the Small Animal Imaging Facility; N. Kosovilka in the Stanford PAN Facility; Y. Rosenberg-Hasson in the Stanford Human Immune Monitoring Center; R. H. Dauskardt and the graduate students in the Department of Materials Science and Engineering (M. Giachino, J. Yang, S. Isaacson, and K. Biniek) for their assistance with MST; T. Naik, K. Penner, and J. Duncan for technical assistance; and S. Djomehri and S. Ho in the Division of Biomaterials and Bioengineering at the University of California, San Francisco for their assistance with μCT.

Funding: This study was supported by the NIH (grants R56 DE025597, R01 DE021683, R21 DE024230, R01 DE019434, RC2 DE020771, U01 HL099776, and R21 DE019274 to M.T.L.; grants U01HL099999, 5 R01

CA86065, and 5 R01 L058770 to L.L.W.; and grants R01 and DE024772 to F.Y); Siebel Fellowship from Thomas and Stacey Siebel Foundation, Prostate Cancer Foundation Young Investigator Award, and the National Institute on Aging Research Career Development Award (grant 1K99AG049958-01A1) (to C.K.F.C); California Institute for Regenerative Medicine (CIRM) (grant TR1-01249), the Oak Foundation, the Hagey Laboratory for Pediatric Regenerative Medicine, and the Gunn/Olivier Research Fund (to M.T.L.); CIRM grant TR3-05569) and NSF CAREER award program (CBET-1351289) (to F.Y.); Stanford University Transplant and tissue Engineering Center of Excellence Fellowship (to A. McArdle and R.T.); and the Plastic Surgery Foundation/Plastic Surgery Research Council Pilot Grant and the American Society of Maxillfacial Surgeons Research Grant (to R.T.)

REFERENCES AND NOTES

1. Danaei G, Finucane MM, Lu Y, Singh GM, Cowan MJ, Paciorek CJ, Lin JK, Farzadfar F, Khang YH, Stevens GA, Rao M, Ali MK, Riley LM, Robinson CA, Ezzati M. Global burden of metabolic risk factors of chronic diseases collaborating, national, regional, and global trends in fasting plasma glucose and diabetes prevalence since 1980: Systematic analysis of health examination surveys and epidemiological studies with 370 country-years and 2.7 million participants. Lancet. 2011; 378:31–40. [PubMed: 21705069]
2. Gregg EW, Xzhuo, Cheng YJ, Albright AL, Narayan KMV, Thompson TJ. Trends in lifetime risk and years of life lost due to diabetes in the USA. 1985–2011: A modelling study. Lancet Diabetes Endocrinol. 2014; 2:867–874. [PubMed: 25128274]
3. Lipscombe LL. The US diabetes epidemic: Tip of the iceberg. Lancet Diabetes Endocrinol. 2014; 2:854–855. [PubMed: 25128273]
4. Ai-Aql ZS, Alagl AS, Graves DT, Gerstenfeld LC, Einhorn TA. Molecular mechanisms controlling bone formation during fracture healing and distraction osteogenesis. J Dent Res. 2008; 87:107–118. [PubMed: 18218835]
5. Einhorn TA, Gerstenfeld LC. Fracture healing: Mechanisms and interventions. Nat Rev Rheumatol. 2015; 11:45–54. [PubMed: 25266456]
6. Macey LR, Kana SM, Jingushi S, Terek RM, Borretos J, Bolander ME. Defects of early fracture-healing in experimental diabetes. J Bone Joint Surg Am. 1989; 71:722–733. [PubMed: 2659600]
7. Montagnani A, Gonnelli S, Alessandri M, Nuti R. Osteoporosis and risk of fracture in patients with diabetes: An update. Aging Clin Exp Res. 2011; 23:84–90. [PubMed: 21743287]
8. Moseley KF. Type 2 diabetes and bone fractures. Curr Opin Endocrinol Diabetes Obes. 2012; 19:128–135. [PubMed: 22262002]
9. Chan CK, Seo EY, Chen JY, Lo D, McArdle A, Sinha R, Tevlin R, Seita J, Vincent-Tompkins J, Wearda T, Lu W-J, Senarath-Yapa K, Chung MT, Marecic O, Tran M, Yan KS, Upton R, Walmsley GG, Lee AS, Sahoo D, Kuo CJ, Weissman IL, Longaker MT. Identification and specification of the mouse skeletal stem cell. Cell. 2015; 160:235–298.
10. Marecic O, Tevlin R, McArdle A, Seo EY, Wearda T, Duldulao C, Walmsley GG, Nguyen A, Weissman IL, Chan CKF, Longaker MT. Identification and characterization of an injury-Induced skeletal progenitor. Proc Natl Acad Sci USA. 2015; 112:9920–9925. [PubMed: 26216955]
11. Fajardo RJ, Karim L, Calley VI, Bouxsein ML. A review of rodent models of type 2 diabetic skeletal fragilily. J Bone Miner Res. 2014; 29:1025–1040. [PubMed: 24585709]
12. Thomas T, Burguera B. Is leptin the link between fat and bone mass? J Bone Miner Res. 2002; 17:1563–1569. [PubMed: 12211425]
13. Ducy P, Amling M, Takeda S, Priemel ML, Schilling AF, Beil FT, Shen J, Vinson C, Reuger JM, Karsenty G. Leptin inhibits bone formation through a hypothalamic relay: A central control of bone mass. Cell. 2000; 100:197–207. [PubMed: 10660043]
14. Chan CKF, Lindau P, Jiang W, Chen JY, Zhang LF, Chen CC, Seita J, Sahoo D, Kim JB, Lee A, Park S, Nag D, Gong Y, Kulkarni S, Luppen CA, Theologis AA, Wan DC, DeBoer A, Seo EY, Vincent-Tompkins JD, Loh K, Walmsley GG, Kraft DL, Wu JC, Longaker MT, Weissman IL. Clonal precursor of bone, cartilage, and hematopoietic niche stromal cells. Proc Natl Acad Sci USA. 2013; 110:12643–12648. [PubMed: 23858471]
15. Baht GS, Silkstone D, Vi L, Nadesan P, Amani Y, Whetstone H, Wei Q, Alman BA. Exposure to a youthful circulation rejuvenates bone repair through modulation of beta-catenin. Nat Commun. 2015; 6:7131. [PubMed: 25988592]

16. Pietramaggiori G, Scherer SS, Alperovich M, Chen B, Orgill DP, Wagers AJ. Improved cutaneous healing in diabetic mice exposed to healthy peripheral circulation. J Invest Dermatol. 2009; 129:2265–2274. [PubMed: 19295612]

17. Chan CK, Chen C-C, Luppen CA, Kim JB, DeBoer AT, Wei K, Heims JA, Kuo CJ, Kralt DL, Weissman IL. Endochondral ossification is required for haematopoietic stem-cell niche formation. Nature. 2009; 457:490–494. [PubMed: 19078959]

18. Seita J, Sahoo D, Rossi DJ, Bhattacharya D, Serwold T, Inlay MA, Ehrlich LI, Fathman JW, Dill D, Weissman IL. Gene expression commons: An open platform for absolute gene expression profiling. PLOS ONE. 2012; 7:e40321. [PubMed: 22815738]

19. Chung, U-i, Schipani, E., McMahon, AP., Kronenberg, HM. *Indian hedgehog* couples chondrogenesis to osteogenesis in endochondral bone development. J Clin Invest. 2001; 107:295–304. [PubMed: 11160153]

20. Hojo H, Ohba S, Yano F, Saito T, Ikeda T, Nakajima K, Komiyama Y, Nakagata N, Suzuki K, Takato T, Kawaguchi U-i, Chung M. Glil protein participates in Hedgehog-mediated specification of osteoblast lineage during endochondral ossification. J Biol Chem. 2012; 287:17860–17869. [PubMed: 22493482]

21. Karp SJ, Schipani E, St-Jacques B, Hunzelman J, Kronenberg H, McMahon AP. Indian hedgehog coordinates endochondral bone growth and morphogenesis via parathyroid hormone related-protein-dependent and -independent pathways. Development. 2000; 127:543–548. [PubMed: 10631175]

22. Lin Y-C, Roflller SR, Yan Y-T, Yang R-B. Disruption of Scube2 impairs endochondral bone formation. J Bone Miner Res. 2015; 30:1255–1267. [PubMed: 25639508]

23. Sacchetti B, Funari A, Michienzi S, Di Cesare S, Piersanti S, Saggio I, Tagliafico E, Ferrari S, Robey PG, Riminucci M, Bianco P. Self-renewing osteoprogenitors in bone marrow sinusoids can organize a hematopoietic microenvironment. Cell. 2007; 131:324–336. [PubMed: 17956733]

24. Levi B, Hyun JS, Montoro DD, Lo DT, Chan CKF, Hu S, Sun N, Lee M, Grova M, Connolly AJ, Wu JC, Gurtner GC, Weissman IL, Wan DC, Longaker MT. In vivo directed differentiation of pluripotent stem cells for skeletal regeneration. Proc Natl Acad Sci USA. 2012; 109:20379–20384. [PubMed: 23169671]

25. Conboy IM, Conboy MJ, Wagers AJ, Girma ER, Weissman IL, Rando TA. Rejuvenation of aged progenitor cells by exposure to a young systemic environment. Nature. 2005; 433:760–764. [PubMed: 15716955]

26. Loffredo FS, Steinhauser ML, Jay SM, Gannon J, Pancoast JR, Yalamanchi P, Sinha M, Dall'Osso C, Khong D, Shadrach JL, Miller CM, Singer BS, Stewart A, Psychogios N, Gerszten RE, Hartigan AJ, Kim MJ, Serwold T, Wagers AJ, Lee RT. Growth differentiation factor 11 is a circulating factor that reverses age-related cardiac hypertrophy. Cell. 2013; 153:828–839. [PubMed: 23663781]

27. Villeda SA, Plambeck KE, Middeldorp J, Castellano JM, Mosher KI, Luo J, Smith LK, Bieri G, Lin K, Berdnik D, Wabl R, Udeochu J, Wheatley EG, Zou B, Simmons DA, Xie XS, Longo FM, Wyss-Coray T. Young blood reverses age-related impairments in cognitive function and synaptic plasticity in mice. Nat Med. 2014; 20:659–663. [PubMed: 24793238]

28. Hilton MJ, Tu X, Cook J, Hu H, Long F. Ihh controls cartilage development by antagonizing Gli3 but requires additional effectors to regulate osteoblast and vascular development. Development. 2005; 132:4339–4351. [PubMed: 16141219]

29. Hotamisligil GS, Shargill NS, Spiegelman BM. Adipose expression of tumor necrosis factor-α: Direct role in obesity-linked insulin resistance. Science. 1993; 259:87–91. [PubMed: 7678183]

30. Hotamisligil GS, Budavari A, Murray D, Spiegelman BM. Reduced tyrosine kinase activity of the insulin receptor in obesity-diabetes. Central role of tumor necrosis factor-α. J Clin Invest. 1994; 94:1543–1549. [PubMed: 7523453]

31. Hotamisligil GS, Amer P, Caro JF, Atkinson RL, Spiegelman BM. Increased adipose tissue expression of tumor necrosis factor-α in human obesity and insulin resistance. J Clin Invest. 1995; 95:2409–2415. [PubMed: 7738205]

32. Moller DE. Potential role of TNF-α in the pathogenesis of insulin resistance and type 2 diabetes. Trends Endcrinol Metab. 2000; 11:212–217.

33. Kayal RA, Siqueira M, Alblowi J, McLean J, Krothapalli N, Faibish D, Einhorn TA, Gerstenfeld LC, Graves DT. TNF-α mediates diabetes-enhanced chondrocyte apoptosis during fracture healing and stimulates chondrocyte apoptosis through FOXOl. J Bone Miner Res. 2010; 25:1604–1615. [PubMed: 20200974]
34. Alblowi J, Kayal RA, Siqueira M, McKenzie E, Krothapalli N, McLean J, Conn J, Nikolajczyk B, Einhorn TA, Gerstenfeld L, Graves DT. High levels of tumor necrosis factor-α contribute to accelerated loss of cartilage in diabetic fracture healing. Am J Pathol. 2009; 175:1574–1585. [PubMed: 19745063]
35. Donath MY, Shoelson SE. Type 2 diabetes as an inflammatory disease. Nat Rev Immunol. 2011; 11:98–107. [PubMed: 21233852]
36. Peluso I, Palmery M. The relationship between body weight and inflammation: Lesson from anti-TNF-α antibody therapy. Hum Immunol. 2015; 47:47–53.
37. Gerstenfeld LC, Cho TJ, Kon T, Aizawa T, Tsay A, Fitch J, Barnes GL, Graves DT, Einhorn TA. Impaired fracture healing in the absence of TNF-α signaling: The role of TNF-α in endochondral cartilage resorption. J Bone Miner Res. 2003; 18:1584–1592. [PubMed: 12968667]
38. Kayal RA, Tsatsas D, Bauer MA, Allen B, Al-Sebaei MO, Kakar S, Leone CW, Morgan EF, Gerstenfeld LC, Einhorn TA, Graves DT. Diminished bone formation during diabetic fracture healing is related to the premature resorption of cartilage associated with increased osteoclast activity. J Bone Miner Res. 2007; 22:560–568. [PubMed: 17243865]
39. He H, Liu R, Desta T, Leone C, Gerstenfeld LC, Graves DT. Diabetes causes decreased osteoclastogenesis, reduced bone formation, and enhanced apoptosis of osteoblastic cells in bacteria stimulated bone loss. Endocrinology. 2004; 145:447–452. [PubMed: 14525917]
40. Li L, Cheng WY, Glicksberg BS, Gottesman O, Tamler R, Chen R, Bottinger EP, Dudley JT. Identification of type 2 diabetes subgroups through topological analysis of patient similarity. Sci Transl Med. 2015; 7:311ra174.
41. Hasegawa H, Ozawa S, Hashimoto K, Takeichi T, Ogawa T. Type 2 diabetes impairs implant osseointegration capacity in rats. Int J Oral Maxillofac Implants. 2008; 23:237–246. [PubMed: 18548919]
42. Djomehri SI, Candell S, Case T, Browning A, Marshall GW, Yun W, Lau SH, Webb S, Ho SP. Mineral density volume gradients in normal and diseased human tissues. PLOS ONE. 2015; 10:e0121611. [PubMed: 25856386]

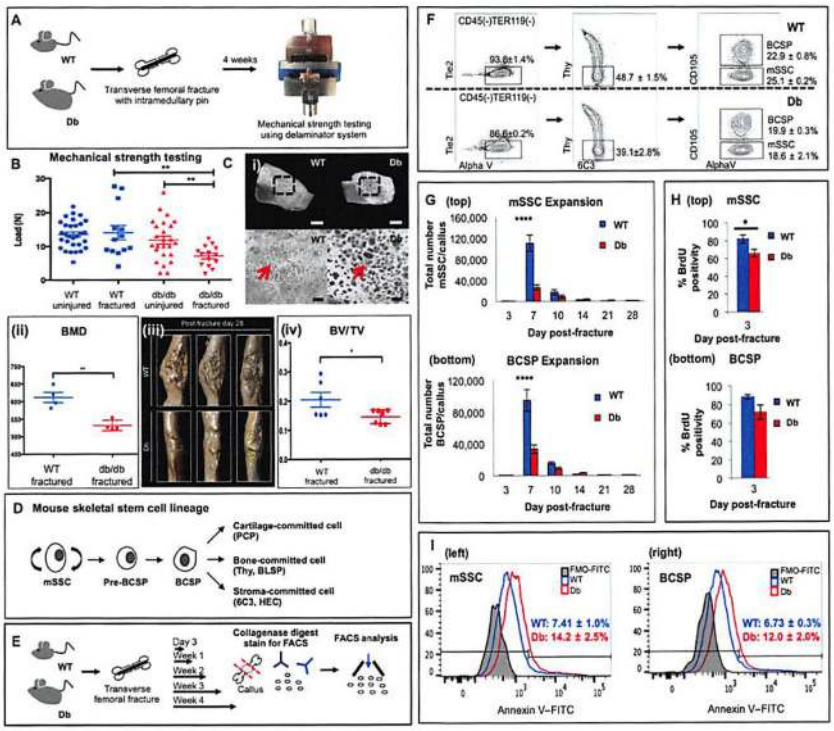

Fig. 1. mSSC-dependent bone healing is impaired in Db mice

(A) Schematic of fracture creation and assessment by MST. (**B**) Maximal load to fracture (in newtons) of uninjured and healing femora from Leprdb (db/db, DbLR, or Db; red) versus wild-type (WT; blue) mice [$n = 13$ to 24; $^{**}P = 0.0018$, one-way analysis of variance (ANOVA)]. (**C**) (i) Representative μCT images showing trabecular bone of healing femora from WT (left column) or DbLR (right column) mice. The Outlined area is magnified showing differences in trabecular spaces (red arrows). Scale bars, 500 μm (top) and 100 μm (bottom). (ii) Assessment of bone mineral density (BMD) of trabecular bone in healing femora from WT versus DbLR mice ($n = 4$). (iii) μCT images of calluses from WT and DbLR mice. (iv) Assessment of bone volume/total volume (BV/TV) of healing femora from WT or DbLR mice ($n = 6$ to 7). (**D**) Schematic of mSSC lineage hierarchy: mSSC; pre-bone cartilage, stromal progenitor (Pre-BCSP); BCSP; pro-chondrogenic cell (PCP); Thy^{+} osteogenic progenitor (Thy); B cell lymphocyte stromal progenitor (BLSP); $6C3^{+}$ stromal progenitor (6C3); hepatic leukemia factor-expressing cell (HEC). (**E**) Schematic of stem and progenitor cell isolation. mSSCs and BCSPs were isolated from whole uninjured femora and whole calluses at different time points using fluorescence-activated cell sorting (FACS). (**F**) FACS plots showing similar proportions of mSSCs and BCSPs in post-fracture day 7 calluses from WT (top row) versus DbLR (bottom row) mice. (**G**) Temporal differences in absolute cell numbers of mSSCs (top) and BCSPs (bottom) in WT versus DbLR mice ($n = 5$ per group). (**H**) Respective population percentages of 5-bromo-2′-deoxyuridine (BrdU)-labeled mSSCs (top) or BCSPs (bottom) from post-fracture day 3 calluses ($n = 5$ per group). (**I**) Respective population percentages of annexin V expression in mSSCs (left) and BCSPs (right) from post-fracture day 7 calluses of DbLR versus WT mice. FMO, full minus one stain; FITC, fluorescein isothiocyanate. Data and error bars represent means ± SEM. $^{*}P < 0.05$, $^{**}P < 0.001$, $^{****}P < 0.0001$, unpaired two-tailed t test.

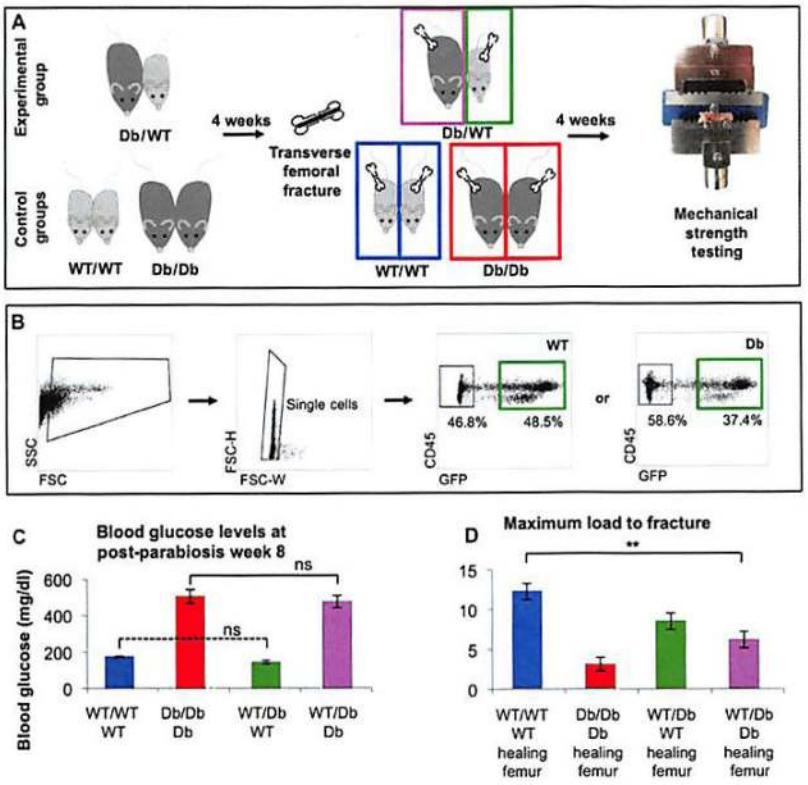

Fig. 2. Exposure to a non-Db circulation does not fully restore Db fracture healing

(**A**) Schematic of parabiotic pairing, fracture creation, and assessment of healing using MST. Parabionts were rested for 4 weeks before further testing to ensure blood chimerism. Fractures were fixed with an intramedullary pin. (**B**) Representative FACS analysis confirming blood chimerism in parabiotic pairs. Blood chimerism was determined by WT green fluorescent protein-expressing (GFP^+, green boxes) cells in nonfluorescent DbLR mice, (**C**) Blood glucose levels of each mouse in a chimeric pair at post-parabiosis week 8 show that parabiosis does not change the glycemic control of DbLR or WT mice in WT/DbLR chimeric pairs ($n = 5$ per group), (**D**) MST of healing femora from each parabiotic pair shows that a non-Db circulation increases the strength of DbLR femora but does not restore it to WT levels ($n = 5$ per group: $^{**}P = 0.0014$, one-way ANOVA). Data and error bars represent means ± SEM. $^{**}P < 0.01$, unpaired two-tailed t test.

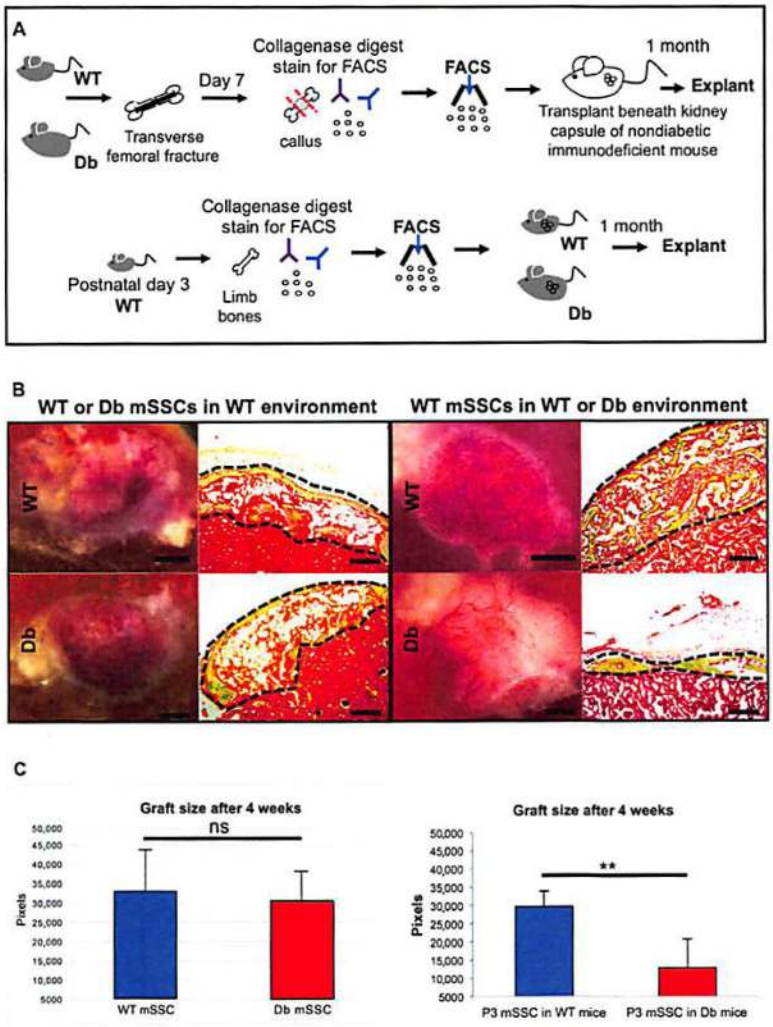

Fig. 3. Altered mSSC skeletogenic activity is cell-extrinsic in Db mice

(**A**) Schematic of kidney capsule transplantation assays. FACS-sorted mSSCs (2×10^4) from WT or DbLR calluses (top sequence) or from the appendicular skeleton of postnatal day 3 (P3) mice (bottom sequence) were transplanted into non-Db, immunodeficient (top) and WT or DbLR (bottom) mice. Heterotopic skeletal grafts were excised after 1 month for histological analysis. (**B**) Left: Representative micrographs of grafts produced in immunocompromised mice by mSSCs from WT (top row) or DbLR (bottom row) mice show no difference in graft size (scale bars, 1 mm; left column) or tissue composition (scale bars, 200 μm; right column). Right: Grafts produced in WT (top row) or DbLR (bottom row) mice by P3 mSSCs show no significant differences in graft size [scale bars, 1 mm (left column) and 200 μm (right column)]. Movat's pentachrome stain: yellow, bone; blue, cartilage; brown, marrow; red, kidney tissue. (**C**) Quantification of kidney graft histomorphometry ($n = 4$ per group). Data and error bars represent means ± SEM. $^{**}P < 0.01$, unpaired two-tailed t test.

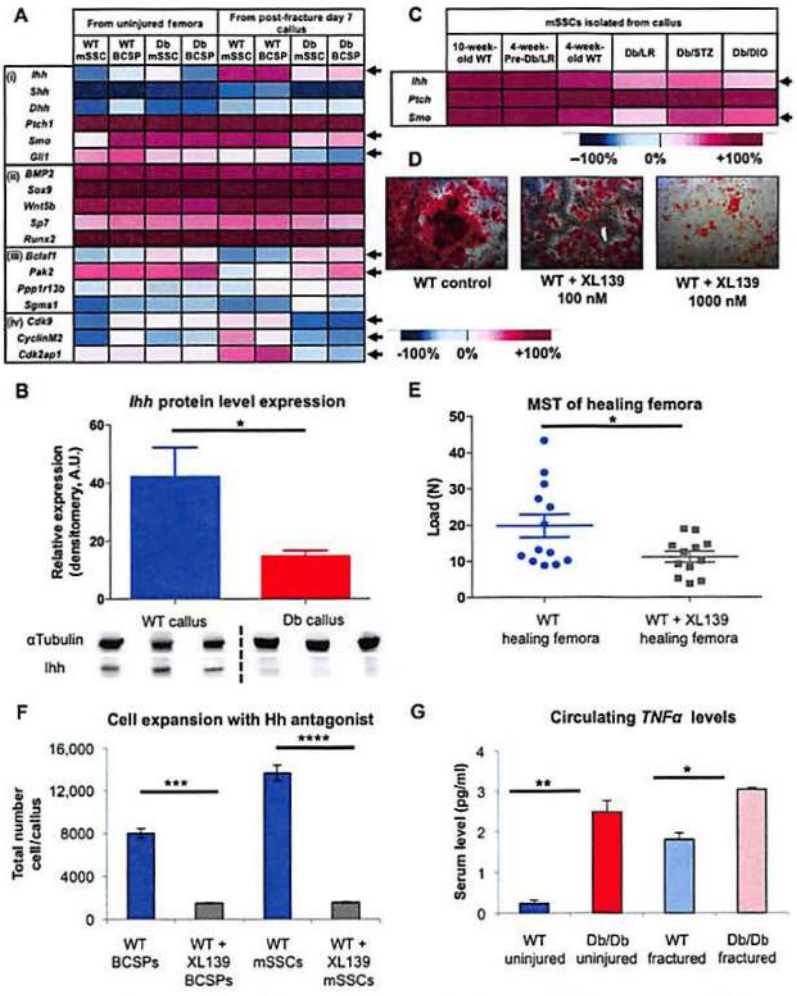

Fig. 4. Db skeletal niches exhibit differential Hh signaling after fracture

(**A**) Heat map showing relative gene expression of skeletogenic factors in mSSCs and BCSPs from uninjured femora (left columns) or calluses (right columns) of WT versus DbLR mice. Genes related to (i) Hh signaling; (ii) skeletal development, growth, and repair; (iii) apoptotic processes; and (iv) proliferation are shown. Differential gene expression was seen for Hh signaling factors, apoptosis-related proteins, and proliferation-related proteins (black arrows). Blue, low expression; red, high expression. (**B**) Relative protein levels of Ihh in post-fracture day 7 calluses from DbLR versus WT mice. Western blot quantification determined by densitometry analysis ($n = 8$). A.U., arbitrary units. (**C**) Heat map showing relative gene expression of Hh signaling factors in mSSCs from post-fracture day 7 calluses of multiple Db and control mouse models. Models Include 10-week-old WT, 4-week-old pre-Db Leprdb (pre-DbLB), 4-week-old WT Leprdb (DbLR), streptozotocin-induced diabetes (DbSTZ), and diet-induced diabetes (DbDIO). Black arrows mark differentially expressed genes. (**D**) Alizarin red staining shows that XL139 reduces in vitro osteogenic potential of WT mSSCs from post-fracture day 7 calluses in a dose-dependent manner. (**E**) MST of healing femora at post-fracture week 4 from XL139-treated (gray) versus untreated (blue) WT mice ($n = 12$ to 13). (**F**) Absolute cell numbers of WT mSSCs and BCSPs from

XL139-treated versus untreated post-fracture day 7 calluses ($n = 5$). (**G**) Pre- and post-fracture serum levels of TNFα in DbLR versus WT mice ($n = 3$). Data and error bars represent means ± SEM. *$P < 0.05$, **$P < 0.001$, ***$P < 0.001$, ****$P < 0.0001$, unpaired two-tailed *t* test.

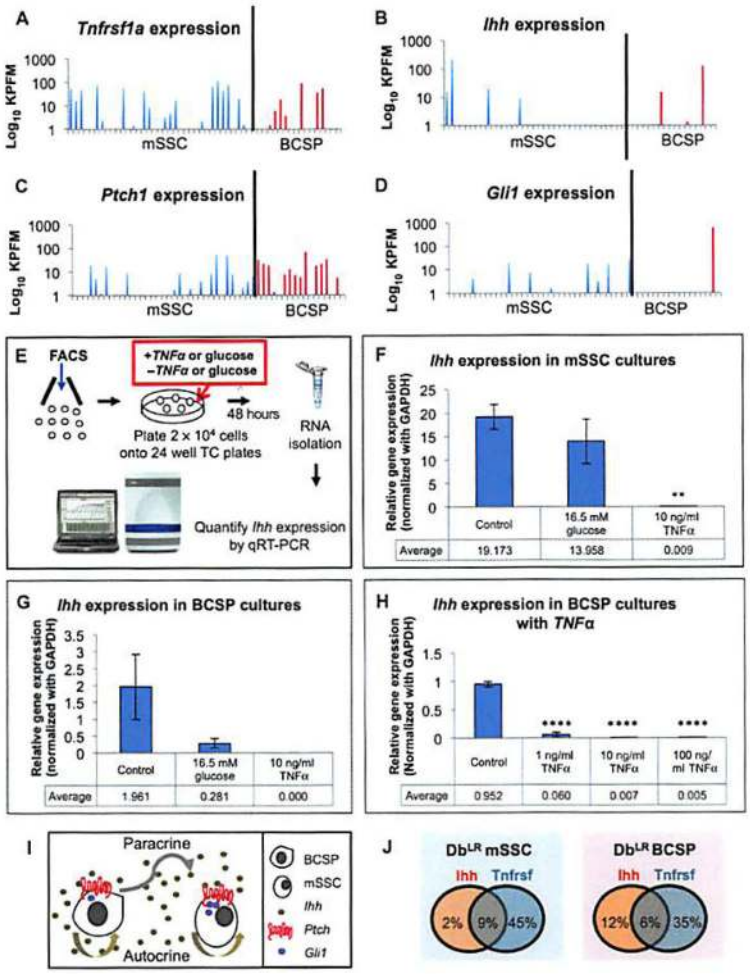

Fig. 5. Increased levels of TNFα directly suppress Ihh expression in skeletal progenitors

(**A**) scRNA-seq shows cell-specific expression of TNFα receptor, TNF receptor superfamily 1α (Tnfrsf1α), in mSSCs and BCSPs from post-fracture day 7 calluses of DbLR mice. (**B**) scRNA-seq shows cell-specific expression of Ihh in mSSCs and BCSPs from post-fracture day 7 calluses of DbLR mice. (**C**) scRNA-seq shows cell-specific expression of Hh receptor, Ptch1, in mSSCs and BCSPs from post-fracture day 7 calluses of DbLR mice. (**D**) scRNA-seq shows cell-specific expression of Hh effector, Gli1, in mSSCs and BCSPs from post-fracture day 7 calluses of DbLR mice. (**E**) Schematic of procedure investigating the effects of glucose or TNFα on Ihh expression in vitro. FACS-sorted mSSCs and BCSPs were isolated from the appendicular skeleton of uninjured P3 WT mice. Protein quantification was measured using qRT-PCR. (**F**) qRT-PCR analysis shows that TNFα significantly diminishes Ihh expression in mSSC-derived cultures isolated from uninjured P3 mice. GAPDH, glyceraldehyde-3-phosphate dehydrogenase. (**G**) qRT-PCR analysis shows that glucose and TNFα reduce Ihh expression in BCSP-derived cultures isolated from uninjured P3 mice. (**H**) qRT-PCR analysis shows that TNFα diminishes Ihh expression in BCSP-derived cultures isolated from uninjured P3 mice in a dose-dependent manner. (**I**) Schematic of stem and progenitor cell cross-talk in the skeletal niche. BCSPs mediate mSSC activity

through autocrine and/or paracrine signaling. Ihh expressed by BCSPs is recognized by Ptch1 on mSSCs, leading to signal transduction via Gli1. (**J**) Venn diagram of Ihh/Tnfrsf coexpression in DbLR mSSCs (left) and BCSPs (right) from post-fracture day 7 calluses shows that either autocrine or paracrine Ihh-mediated signaling could be repressed directly via TNFα signaling. Data and error bars represent means ± SEM. $^{**}P < 0.01$, $^{****}P < 0.0001$, unpaired two-tailed *t* test.

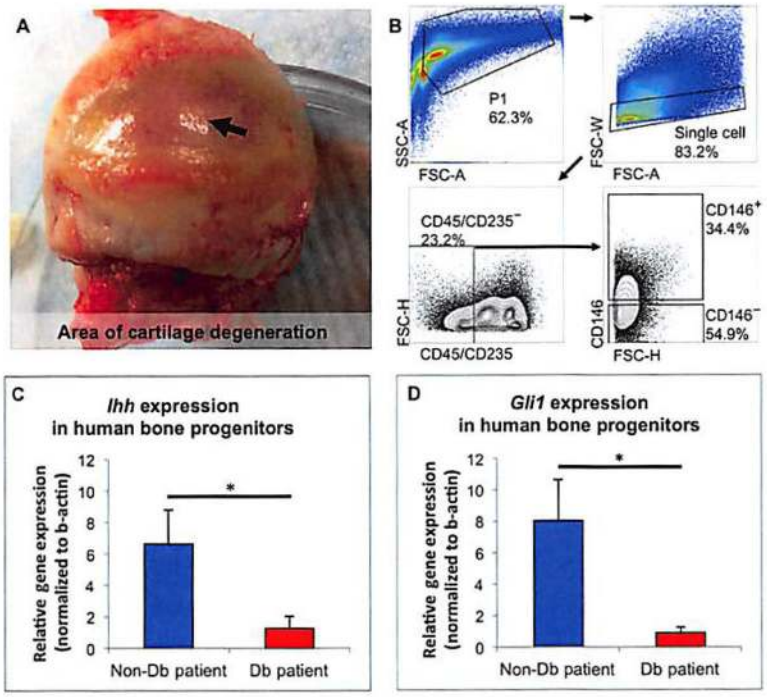

Fig. 6. Ihh and Gli1 expression are repressed in Db human skeletal progenitors

(**A**) Representative image of osteoarthritic femoral head, with black arrow marking an area of cartilage degeneration from which cells were isolated for analysis. (**B**) FACS gating strategy to isolate human skeletal progenitor populations from collagenase-dissociated cells extracted from human femoral head and knee specimens. Both $CD146^{+}$ and $CD146^{-}$ skeletal progenitors are represented in nonhematopoietic $CD45^{-}CD235^{-}$ populations. (**C**) qRT-PCR analysis of relative Ihh expression in $CD45^{-}CD235^{-}CD146^{+/-}$ human skeletal progenitors from non-Db versus Db patients ($n = 5$ to 6). (**D**) qRT-PCR analysis of relative Gli1 expression in $CD45^{-}CD235^{-}CD146^{+/-}$ human skeletal progenitors from non-Db versus Db patients ($n = 5$ to 6). Data and error bars represent means ± SEM. $^{*}P < 0.05$, unpaired two-tailed *t* test.

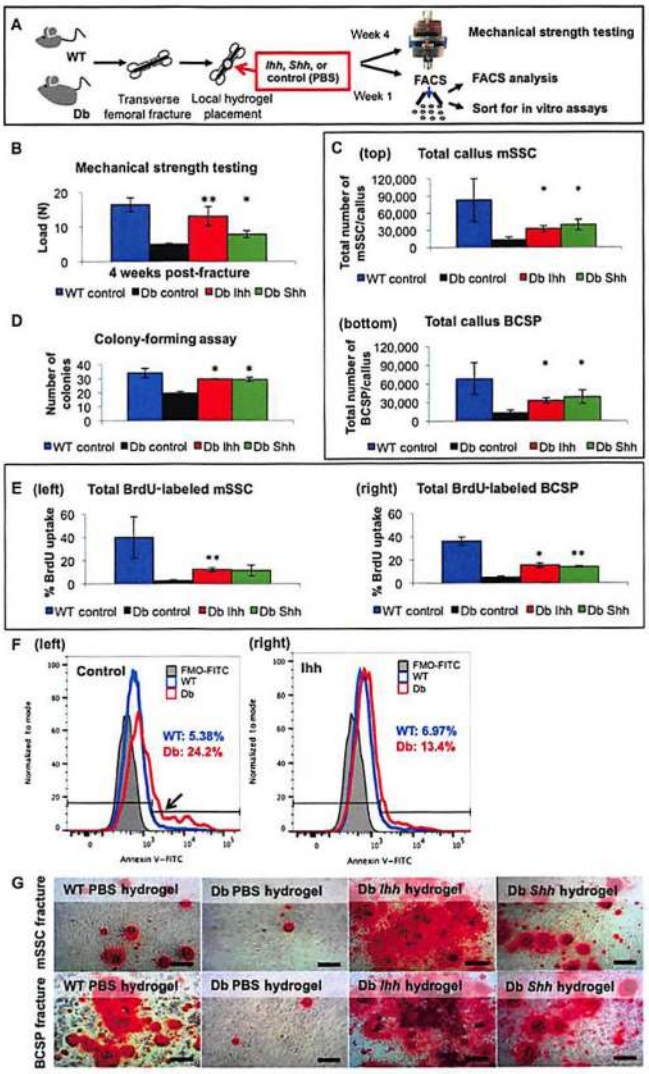

Fig. 7. Local delivery of Ihh restores the mSSC injury response

(**A**) Schematic of slow-release hydrogel placement on the fracture site in WT or DbLR mice. Hydrogel-treated mSSCs and BCSPs were isolated from post-fracture day 7 calluses using FACS for in vitro analyses, or post-fracture week 4 femora were harvested for MST. (**B**) MST of PBS-treated WT femora (blue) versus PBS-treated (black), Ihh-treated (red), or Shh-treated (green) femora from DbLR mice. Ihh or Shh treatment significantly increases DbLR femur strength compared to PBS-treated controls ($n = 5$). (**C**) Absolute cell numbers of mSSCs (top) and BCSPs (bottom) from PBS-treated WT femora versus PBS-, Ihh-, or Shh-treated calluses from DbLR mice. Calluses were harvested at post-fracture day 7 ($n = 5$). (**D**) Colony-forming assay of mSSCs isolated at post-fracture day 7 from each experimental group. The total number of colonies was measured ($n = 3$). (**E**) Respective population percentages of BrdU-labeled post-fracture day 3 callus mSSCs (left) or BCSPs (right) from each experimental group ($n = 4$). (**F**) Respective population percentages of annexin V expression in mSSCs from PBS-treated (left column) versus Ihh-treated (right column) calluses of WT (blue) or DbLR (red) mice. Calluses harvested at post fracture day

7. (**G**) Alizarin red staining shows osteogenic potential of mSSCs (top row) and BCSPs (bottom row) from PBS-treated WT (far left column) and PBS-treated (second column from left), Ihh-treated (second column from right), or Shh-treated (far right column) Db calluses. mSSCs and BCSPs were isolated from DbLR mice at post-fracture day 7. Bright-field microscopy, 10×. Scale bars, 200 μm. Data and error bars represent means ± SEM. $*P < 0.05$, $**P < 0.01$, unpaired two-tailed *t* test.

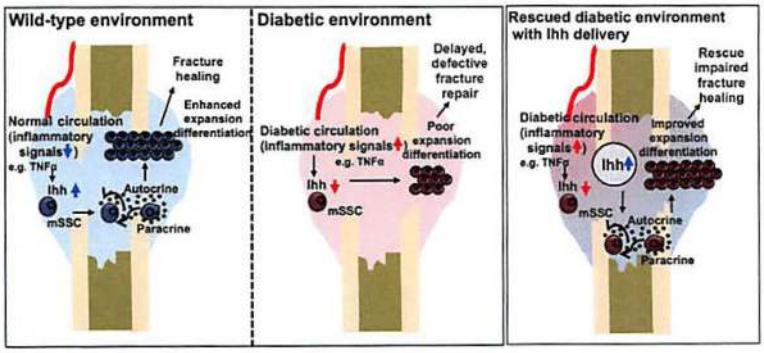

Fig. 8. Schematic showing the cellular and molecular mechanisms underlying impaired Db skeletal repair

(**Left**) In non-Db conditions, normal Hh-mediated cross-talk between mSSCs and BCSPs in skeletal niches coordinates an effective injury response. (**Top right**) in Db conditions, high serum levels of TNFα disrupt skeletal niche signaling, leading to impaired fracture repair. (**Bottom right**) Impaired fracture repair in Db conditions Can be rescued by supplying Ihh signaling.